

# CameraCtrl: Enabling Camera Control for Text-to-Video Generation

Hao He<sup>1</sup>, Yinghao Xu<sup>3</sup>, Yuwei Guo<sup>1</sup>,  
Gordon Wetzstein<sup>3</sup>, Bo Dai<sup>2</sup>, Hongsheng Li<sup>1</sup>, and Ceyuan Yang<sup>2</sup>

<sup>1</sup> The Chinese University of Hong Kong

<sup>2</sup> Shanghai Artificial Intelligence Laboratory

<sup>3</sup> Stanford University

**Abstract.** Controllability plays a crucial role in video generation since it allows users to create desired content. However, existing models largely overlooked the precise control of camera pose that serves as a cinematic language to express deeper narrative nuances. To alleviate this issue, we introduce **CameraCtrl**, enabling accurate camera pose control for text-to-video (T2V) models. After precisely parameterizing the camera trajectory, a plug-and-play camera module is then trained on a T2V model, leaving others untouched. Additionally, a comprehensive study on the effect of various datasets is also conducted, suggesting that videos with diverse camera distribution and similar appearances indeed enhance controllability and generalization. Experimental results demonstrate the effectiveness of **CameraCtrl** in achieving precise and domain-adaptive camera control, marking a step forward in the pursuit of dynamic and customized video storytelling from textual and camera pose inputs. Our project website is at: <https://hehao13.github.io/projects-CameraCtrl/>.

**Keywords:** Camera control · Video generation

## 1 Introduction

Recently, diffusion models have significantly advanced video generation [7, 16, 19, 47, 48], revolutionizing digital content design workflows. Controllability plays a crucial role in practical video generation applications, allowing for better customization according to user needs. This enhances the quality, realism, and usability of the generated videos. While text and image inputs are commonly used for achieving controllability, they may lack precise control over content and motion. To address this, some approaches have been proposed, leveraging control signals such as optical flow [12, 52], pose skeleton [32, 39], and other multi-modal signals [37, 45], enabling more accurate control for guiding video generation.

However, existing models lack precise control over adjusting or simulating camera viewpoints in video generation. The ability to control the camera is crucial not only for enhancing the realism of generated videos but also for increasing user engagement by allowing customized viewpoints. This is particularly important in virtual reality, augmented reality, and game development.

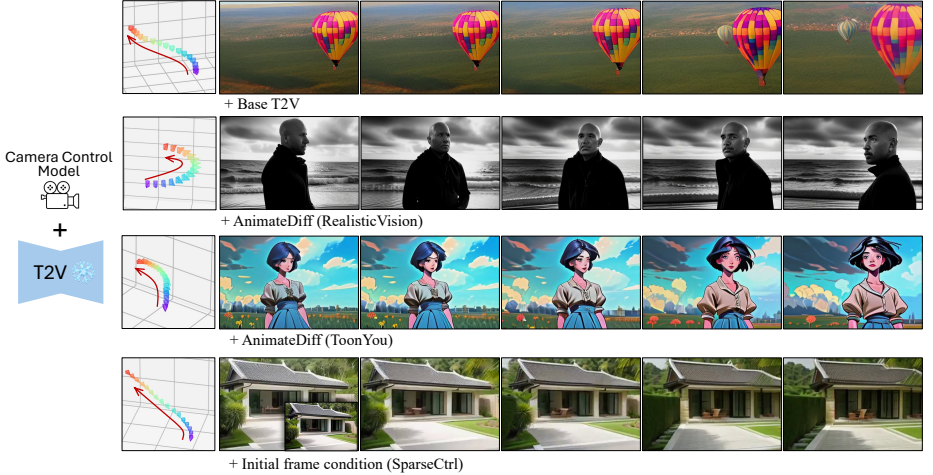


**Fig. 1: Illustration of CameraCtrl.** As a plug-and-play module, it can control the camera trajectory for both general text-to-video generation and personalized one, shown in the first three rows. Additionally, **CameraCtrl** can collaborate with visual controllers, such as the RGB encoder from SparseCtrl [15] to generate videos given the first images while simultaneously managing camera movements. The condition image is in the bottom right corner of the first image in the last row.

Moreover, skillful management of camera movements enables creators to emphasize emotions, highlight character relationships, and guide the audience’s focus, which holds significant value in the film and advertising industries. Recent efforts have been made to introduce camera control in video generation. For example, AnimateDiff [16] incorporates a MotionLoRA module on top of its motion module, enabling specific types of camera movement. Nevertheless, it struggles to generalize to camera trajectories customized by users. MotionCtrl [46] offers more flexible camera control by conditioning its text-to-video (T2V) model on a sequence of camera poses, but relying solely on numerical values without geometric cues of camera parameters may not ensure precise camera control. Additionally, MotionCtrl [46] lacks the capability to generalize camera control across other personalized video generation models.

We thus introduce **CameraCtrl**, learning a precise plug-and-play camera module that could control the camera viewpoints in video generation. Considering that seamlessly integrating a customized camera into existing T2V models is challenging, we investigate how to represent and inject the camera effectively. Concretely, we adopt plücker embeddings [43] as the primary form of camera parameters. This choice is attributed to their encoding of geometric interpretations for each pixel in a video frame, offering a comprehensive description of camera pose information. To ensure the applicability and the generalizability of our **CameraCtrl** after training, we introduce a camera control module that only takes the plücker embedding as input, thus agnostic to the

appearance of the training dataset. To effectively train the camera control model, a comprehensive study is also conducted to investigate how various training data affect from the realistic data to synthetic data. Experimental results suggest that data (*e.g.*, RealEstate10K [57]) with similar appearance to the original base model and diverse camera pose distribution achieves the best trade-off between generalizability and controllability.

We implement our **CameraCtrl** on top of AnimateDiff [16], enabling precise camera control in video generation across various personalized ones, some of which are shown in the first three rows of Fig. 1, demonstrating its versatility and utility in a wide range of video creation contexts. In addition, as shown in the last row of Fig. 1, it is also compatible with other plug-and-play module *e.g.*, SparseCtrl [15] to control viewpoints under the image-to-video settings.

In summary, our main contributions are as follows:

- We introduce **CameraCtrl**, empowering video diffusion models with flexible and precise controllability over camera viewpoints.
- The plug-and-play camera control module can be adapted to various personalized video generation models, producing smooth and visually appealing camera control.
- We provide a comprehensive analysis of datasets to train the camera control module. We hope this will be helpful for future research in this direction.

## 2 Related Work

**Text-to-video generation.** Recent attempts at text-to-video (T2V) generation [11, 18, 22, 25, 38, 55] mainly leverage diffusion models [20, 35, 44] for their stability in training and well-established open-sourced communities. As a pioneer in this field, Video Diffusion Model [21] expands a 2D image diffusion architecture to accommodate video data and jointly train the model on image and video from scratch. To utilize the powerful pre-trained image generator such as Stable Diffusion [36], later works inflate the 2D architecture by interleaving temporal layers between the pre-trained 2D layers and finetune the new model on large video dataset [3]. Among them, Align-Your-Latents [8] efficiently turns T2I into video generators by aligning independently sampled noise maps, while AnimateDiff [16] utilizes a pluggable motion module to enable high-quality animation creation on personalized image backbones [40]. To enhance temporal coherency, Lumiere [5] replaces the commonly used temporal super-resolution module and directly generates full-frame-rate videos. Other significant attempts include leveraging scalable transformer backbone [31], operating in space-temporal compressed latent space, *e.g.*, W.A.L.T. [17] and Sora [10], and using discrete token with language model for video generation [27].

**Controllable video generation.** The ambiguity of solely used text descriptions often leads to weak control for text-to-video models. To provide enhanced guidance, some work with precise signals, *e.g.*, depth/skeleton sequence, to precisely control the scene/human motion in the synthesized videos [13, 15, 24, 26, 49, 56]. Other methods [15, 34] adopt the images as the control signal to the video

generator, contributing to high video quality or accurate temporal relationship modeling.

This paper focuses on camera control during the video generation process. AnimateDiff [16] adopts efficient LoRA [23] finetuning to obtain model weights specified for different shot types. Direct-a-Video [50] proposes a camera embedder to control the camera pose during the video generation process, but it only conditions on three camera parameters, which limits its camera control ability to the most basic types, like pan left. MotionCtrl [46] designs a motion controller that takes more camera parameters as input and produces the corresponding videos with more complex camera poses. However, the necessity to fine-tune part of the video diffusion model’s parameter can hamper its generalization ability. In this study, we aim to control the camera poses during the video generation process precisely, and expect the corresponding camera control model can be used in various personalized video generation models.

### 3 CameraCtrl

Introducing precise control of the camera into existing video generation methods is challenging, but holds significant value in terms of achieving desired results. To accomplish this, we address the problem by considering three key questions: **(1)** How can we effectively represent the camera condition to reflect the geometric movement in 3D space? **(2)** How can we seamlessly inject the camera condition into existing video generators without compromising frame quality and temporal consistency? **(3)** What type of training data should be utilized to ensure proper model training?

This section is thus organized as follows: Sec. 3.1 presents the preliminary of video generation models; Sec. 3.2 introduces the camera representation; Sec. 3.3 presents the camera model  $\Phi_c$  for injecting camera representation into text-to-video (T2V) models. The data selection method is discussed in Sec. 3.4.

#### 3.1 Preliminary of Video Generation

**Text-to-video diffusion models.** Text-to-video (T2V) diffusion models have seen significant advancements in recent years. Some approaches [21, 42] train video generators from scratch, while others [7, 16] utilize powerful text-to-image (T2I) diffusion models. These models often adhere to the original formulation used for image generation. Concretely, a sequence of  $N$  images (or their latent features)  $z_0^{1:N}$  are first added noises  $\epsilon$  gradually to normal distribution at  $T$  steps. Given the noised input  $z_t^{1:N}$ , a neural network  $\hat{\epsilon}_\theta$  is thus trained to predict the added noises. During the training, the network tries to minimize the mean squared error (MSE) between its prediction and the ground truth noise scale; the training objective function is formulated as follows:

$$\mathcal{L}(\theta) = \mathbb{E}_{z_0^{1:N}, \epsilon, c_t, t} [\|\epsilon - \hat{\epsilon}_\theta(z_t^{1:N}, c_t, t)\|], \quad (1)$$

where  $c_t$  represents embeddings of the corresponding text prompts.



**Controllable text-to-video generation.** In the realm of text-to-video generation, there have been further advancements in enhancing controllability. By incorporating additional structural control signals  $s_t$  (e.g., depth maps and canny maps) into the process, controllability for both image and video generation can be enhanced. Typically, these control signals are first fed into an additional encoder  $\Phi_s$  and then injected into the generator through various operations [33, 51, 54]. Consequently, the objective of training this encoder can be defined as follows:

$$\mathcal{L}(\theta) = \mathbb{E}_{z_0^{1:N}, \epsilon, c_t, s_t, t} [\|\epsilon - \hat{\epsilon}_\theta(z_0^{1:N}, c_t, \Phi_s(s_t), t)\|. \quad (2)$$

In this work, we strictly follow this objective to train our camera encoder  $\Phi_c$ .

### 3.2 Representing Camera Condition Effectively

Before diving into the training of the camera encoder, we first investigate which kind of camera representation could precisely reflect the movement in 3D space.

**Camera representation.** Typically, the camera pose refers to the intrinsic and extrinsic parameters, denoted as  $\mathbf{K} \in \mathbb{R}^{3 \times 3}$  and  $\mathbf{E} = [\mathbf{R}; \mathbf{t}]$ , respectively, where  $\mathbf{R} \in \mathbb{R}^{3 \times 3}$  represents the rotation part of the extrinsic parameters, and  $\mathbf{t} \in \mathbb{R}^{3 \times 1}$  is the translation part.

To let a video generator condition on camera pose, one straightforward choice is to feed raw values regarding the camera parameters into the generators. However, such a choice may not contribute to accurate camera control for several reasons: (1) While the rotation matrix  $\mathbf{R}$  is constrained by orthogonality, the translation vector  $\mathbf{t}$  is typically unconstrained in magnitude, leading to a mismatch in the learning process that can affect the consistency of control. (2) Direct use of raw camera parameters makes it difficult for the model to correlate these values with image pixels, limiting precise control over visual details. We thus choose plücker embeddings [43] as the camera pose representation. Specifically, for each pixel  $(u, v)$  in the image coordinate space, its plücker embedding is  $\mathbf{p}_{u,v} = (\mathbf{o} \times \mathbf{d}_{u,v}, \mathbf{d}_{u,v}) \in \mathbb{R}^6$ . Where  $\mathbf{o} \in \mathbb{R}^3$  is the camera center in world coordinate space, which equals to  $\mathbf{t}$ , and  $\mathbf{d}_{u,v} \in \mathbb{R}^3$  is a direction vector in world coordinate space from the camera center to the pixel  $(u, v)$ , it is calculated as,

$$\mathbf{d}_{u,v} = \mathbf{R}\mathbf{K}^{-1}[u, v, 1]^T + \mathbf{t}. \quad (3)$$

Then, it is normalized to ensure it has a unit length. For the  $i$ -th frame in a video sequence, its plücker embedding can be expressed as  $\mathbf{P}_i \in \mathbb{R}^{6 \times h \times w}$ , where  $h$  and  $w$  are the height and width for the frame.

Note that Eq. (3) represents the inverse process of camera projection, which maps point from the 3D world coordinate space into the pixel coordinate system through the use of matrices  $\mathbf{E}$  and  $\mathbf{K}$ . Thus, the plücker embedding has some geometric interpretation for each pixel of a video frame and can provide a more elaborate description of camera pose information. Besides, the value ranges of each item in the plücker embedding are more uniform, which is beneficial for the learning process of the model. After obtaining the plücker embedding  $\mathbf{P}_i$  for the camera pose of the  $i$ -th frame, we represent the entire camera trajectory of

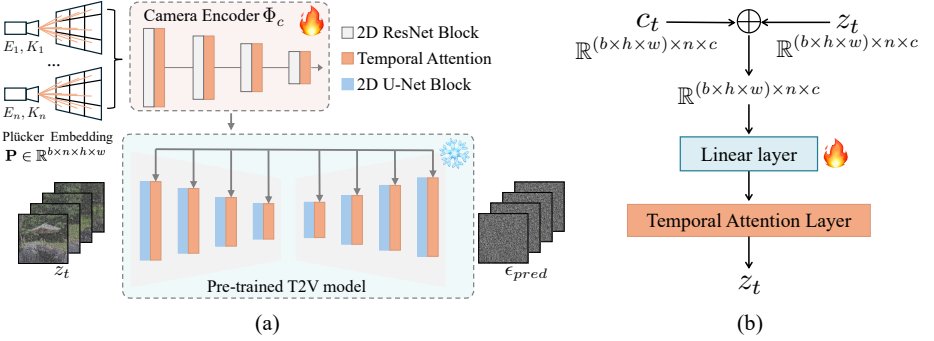


**Fig. 2: Framework of CameraCtrl.** (a) Given a pre-trained T2V model (e.g. AnimateDiff [16]), CameraCtrl trains a camera encoder on it. The camera encoder takes the plücker embedding as input and outputs multi-scale camera representations. These features are then integrated into the temporal attention layers of U-Net at their respective scales to control the video generation process. (b) Details of the camera injection process. The camera features  $c_t$  and the latent features  $z_t$  are first combined through the element-wise addition. A learnable linear layer is adopted to further fuse two representations which are then fed into the first temporal attention layer of each temporal block.

a video as a plücker embedding sequence  $\mathbf{P} \in \mathbb{R}^{n \times 6 \times h \times w}$ , where  $n$  denotes the total number of frames in the video.

### 3.3 Introducing Camera Controllability into Video Generators

As camera trajectory is parameterized into the plücker embedding sequence *i.e.*, spatial maps, we could follow the prior literature [33, 54] by first using an encoder model to extract the camera features and then fusing the camera features into video generators.

**Camera encoder.** Similar to T2I-Adaptor [33], we introduce a camera encoder  $\Phi_c$  specifically designed for videos. This camera encoder includes a temporal attention module after each convolutional block, allowing it to capture the temporal relationships of camera poses throughout the video clip. As is shown in Fig. 2(a),  $\Phi_c$  only takes the plücker embeddings as input and delivers multi-scale features. Through empirical analysis, we observed that using camera conditions along with latent codes, like ControlNet [54], may result in information leakage from the training data, thereby limiting its generalization across various domains.

**Camera fusion.** After obtaining the multi-scale camera features, we aim to integrate these features seamlessly into the U-Net architecture of the T2V model. Thus, we further investigate the fusion of layers in the original video generator, aiming to determine which layers should be used to effectively incorporate the camera information.

Recall that current video generators usually adopt a U-Net-like architecture that contains both spatial and temporal attention. We inject the camera rep-

representations into the temporal attention blocks. This decision stems from the capability of the temporal attention layer to capture temporal relationships, aligning with the inherent sequential and causal nature of a camera trajectory, while the spatial attention layers always picture the individual frames. This camera fusion process is shown in Fig. 2(b). The image latent features  $z_t$  and the camera pose features  $c_t$  are directly combined through pixel-wise addition. Then, this integrated feature is passed through a linear layer, whose output is fed directly into the first temporal attention layer of each motion module.

### 3.4 Learning Camera Distribution in Data-Driven Manner

Training the aforementioned camera encoder on a video generator usually requires a lot of videos with text and camera annotations. One can obtain the camera trajectory through structure-from-motion (SfM) *e.g.*, COLMAP [41] for realistic videos while others could collect videos with ground-truth camera from rendering engine, such as Blender. We thus investigate the effect of various training data on the camera-controlled generator.

**Dataset selection.** We aim to select a dataset with appearances that closely match the training data of the base T2V model and have as wide a camera pose distribution as possible. We choose three datasets as the candidates, they are Objaverse [14], MVImageNet [53], and RealEstate10K [57]. Samples from the three datasets can be found in the supplementary material.

Indeed, datasets generated from virtual engines such as Objaverse [14] exhibit diverse camera distribution since we can control the camera parameters during the rendering process, while it often suffers from a distribution gap in appearance when compared to real-world datasets, such as WebVid-10M [4] which is used to train our base T2V model. When dealing with real-world datasets, such as MVImageNet and RealEstate10K, the distribution of camera parameters is often not very broad. In this case, a balance needs to be found between the complexity of individual camera trajectories and the diversity among multiple camera trajectories. The former ensures that the model learns to control complex trajectories during each training process, while the latter guarantees that the model does not overfit to certain fixed patterns. In reality, while the complexity of camera trajectories in MVImageNet may slightly exceed that of RealEstate10K for individual trajectories, the camera trajectories of MVImageNet are typically limited to horizontal rotations. In contrast, RealEstate10K showcases a wide variety of camera trajectories. Considering our goal to apply the model to a wide range of custom trajectories, we ultimately selected RealEstate10K as our training dataset. Besides, there are some other datasets with characteristics similar to RealEstate10K, such as ACID [30] and MannequinChallenge [29], but their data volume is much smaller than that of RealEstate10K.

**Measuring the camera controllability.** To monitor the training process of our camera encoder, we propose the camera alignment metric to measure the camera control quality by quantifying the error between the input camera conditions and the camera trajectory of generated videos. Concretely, we utilize the COLMAP [41] to extract the camera pose sequence of generated videos,

which consists of the rotation matrixes  $\mathbf{R}_{gen} \in \mathbb{R}^{n \times 3 \times 3}$  and translation vectors  $\mathbf{T}_{gen} \in \mathbb{R}^{n \times 3 \times 1}$  of camera. Furthermore, since the rotation angles and the translation scales are two different mathematical quantities, we measure the angle and error translation errors separately and term them as **RotErr** and **TransErr**. Motivated from [1], the **RotErr** of a generated camera pose sequence is computed by comparing the ground truth rotation matrix  $\mathbf{R}_{gt}$  and  $\mathbf{R}_{gen}$ , formulated as,

$$\text{RotErr} = \sum_{j=1}^n \arccos \frac{\text{tr}(\mathbf{R}_{gen}^j \mathbf{R}_{gt}^{jT}) - 1}{2}, \quad (4)$$

where  $\mathbf{R}_{gt}^j$  and  $\mathbf{R}_{gen}^j$  represent the ground truth rotation matrix and generated rotation matrix for the  $i$ -th frame, respectively. And  $\text{tr}$  is the trace of a matrix. To quantify the translation error, we use the  $L2$  distances between the ground truth translation vector  $\mathbf{T}_{gt}$  and  $\mathbf{T}_{gen}$ , that is,

$$\text{TransErr} = \sum_{j=1}^n \|\mathbf{T}_{gt}^j - \mathbf{T}_{gen}^j\|_2, \quad (5)$$

where  $\mathbf{T}_{gt}^j$  and  $\mathbf{T}_{gen}^j$  is the translation vector for the ground truth camera pose and generated camera pose in the  $j$ -th frame.

## 4 Experiments

In this session, we evaluate **CameraCtrl** with other methods and show its applications in different settings. Sec. 4.1 presents the implementation details. Sec. 4.2 compares **CameraCtrl** with other baseline methods **AnimateDiff** [16] and **MotionCtrl** [46]. Sec. 4.3 shows the comprehensive ablation studies of **CameraCtrl**. Sec. 4.4 express the various applications of **CameraCtrl**.

### 4.1 Implementation details

**T2V base model.** We choose the **AnimateDiff V3** [16] as the base text-to-video (T2V) model and implement our **CameraCtrl** on it. Benefiting from the unique training strategy of **AnimateDiff**, its motion module can be integrated with various text-to-image (T2I) LoRAs, or T2I base models to accommodate the video generation across different domains and genres. This feature helps us in evaluating the generalization ability of our **CameraCtrl**.

**Training.** We use the Adam optimizer to train our model with a constant learning rate of  $1e^{-4}$ . As stated in Sec. 3.4, we choose **RealEstate10K** as the dataset, which has around 65K video clips for training. For the alignment with **AnimateDiff V3**, we train our camera control model at the resolution of  $256 \times 384$ . We take the random horizontal flip as one of the argumentation methods to expand the camera poses. We train the camera encoder and the linear layers for camera feature injection together. We use 16 NVIDIA A100 GPUs to train them with a batch size of 2 per GPU for 50K steps, taking about 1 day.

**Table 1: Quantitative comparisons.** Considering AnimateDiff [16] only supports several basic trajectories (*e.g.*, zoom-in, pan left), we compare against prior work on basic trajectory and random trajectory respectively. **TransErr** and **RotErr** are reported as the metrics.

Method	Basic trajectory		Random trajectory	
	TransErr ↓	RotErr ↓	TransErr ↓	RotErr ↓
AnimateDiff [16]	9.81	1.03	-	-
MotionCtrl [46]	9.02	<b>0.87</b>	13.59	1.41
CameraCtrl (Ours)	<b>8.83</b>	0.95	<b>12.91</b>	<b>1.35</b>

**Evaluation metrics.** To ensure that our camera model does not negatively impact the video generation capabilities of the original T2V model, we utilize the Fréchet Inception Distance (**FID**) to assess the video appearance quality, comparing the generated video quality before and after incorporating the camera model. For our reference videos, we have chosen 1,000 videos from the RealEstate10K test set. Additionally, the quality of camera control is evaluated using the metrics **RotErr** and **TransErr** introduced in the Sec. 3.4.

## 4.2 Comparisons with other methods

To proof the effectiveness and the generalization ability of **CameraCtrl**, we compare it with another two camera control methods: AnimateDiff [16], and MotionCtrl [46]. Despite Direct-a-Video [50] can also be used to control camera pose during the video generation, its model and code are not open source. Given that AnimateDiff supports only eight basic camera trajectories, the comparison between our method and AnimateDiff is limited to these basic trajectories. In contrast, for comparisons with MotionCtrl, besides base camera trajectories, we select 1,000 random camera trajectories from the RealEstate10K test set, generate videos using these trajectories along with their corresponding captions, and subsequently evaluate them using **RotErr** and **TransErr**. Notability, **CameraCtrl** and the MotionCtrl utilize different T2V base models, evaluating the quality of appearance using metrics like FID may not yield accurate comparisons. Therefore, we do not compare these metrics.

The quantitative results are shown in Tab. 1. Compared to MotionCtrl and the MotionLoRA AnimateDiff, it is evident that our approach outperforms AnimateDiff in basic trajectory and MotionCtrl in complex trajectory.

## 4.3 Ablation study

We break down the camera control problem into three challenges, regarding the selection of camera representation in Sec. 3.2, the architecture of camera control model in Sec. 3.3, and the learning process of camera control model in Sec. 3.4. In this session, we comprehensively ablate the design choices to each of them. The rotation error **RotErr** and translation error **TransErr** are evaluated using the

**Table 2: Ablation study** on camera representation, condition injection and effect of various datasets.

Representation type	FID↓	TransErr ↓	RotErr ↓
Raw Values	109.8	14.01	1.41
Raw Values + Plücker embedding	104.3	16.98	1.45
<b>Plücker embedding</b>	<b>100.4</b>	<b>12.91</b>	<b>1.25</b>

(a) How to represent camera parameters.

Attention	FID↓	TransErr ↓	RotErr ↓	Datasets	FID↓	TransErr ↓	RotErr ↓
Spatial Self	108.2	14.52	1.33	Objaverse	165.8	-	-
Spatial Cross	104.3	13.62	1.58	MVImageNet	130.4	13.45	1.31
<b>Temporal</b>	<b>100.4</b>	<b>12.91</b>	<b>1.25</b>	Realestate10K	<b>100.4</b>	<b>12.91</b>	<b>1.25</b>

(b) Where to inject camera representations.

(c) Effect of datasets.

1,000 complex camera trajectories. Besides, to assess the impact of our camera control model to video appearance quality, we measure FID using the original AnimateDiff V3 model, yielding a baseline score 102.3. This score provides a reference for video quality comparison after introducing camera control.

**Plücker embedding represents camera precisely.** Beside plücker embedding to represent the camera parameters, we could directly use the numerical values of camera parameters or a combination of both as a hybrid representations. For the direct use approach, we repeat the 16 camera parameters of each video frame along the spatial dimension. In the hybrid approach, we first repeat the 16 parameters with the aforementioned method then concatenate it with the plücker embedding along the channel dimension. The experimental results are illustrated in Tab. 2a, using the plücker embedding as the camera representation yields the best camera control results, the FID metric is very similar with the reference value 102.2, yielding no loss of appearance. These quantitative results further confirm our intuition in Sec. 3.2 that plücker embedding enables more precise camera control. This accuracy stems from plücker embedding’s ability to provide a geometric interpretation for every pixel. Incorporating original numerical values directly with plücker embedding could compromise this geometric interpretation. Moreover, relying solely on numerical values might lead to numerical mismatches, adversely affecting the camera model’s learning efficiency.

**Noised latents as input limit the generalization.** In ablating the architecture of camera encoders, we differentiate between ControlNet [54], whose input is the summation of image features and plücker embedding, and the T2I-Adaptor, solely using plücker embedding as input. This distinction is crucial as the use of noised latent, mentioned in SparseCtrl [15], has been associated with appearance leakage, effectively limiting the generalization capability of the model. Besides, to enhance inter-frame camera coherence, we also consider adding a temporal attention block to each encoder. Thus, Our experiment covers

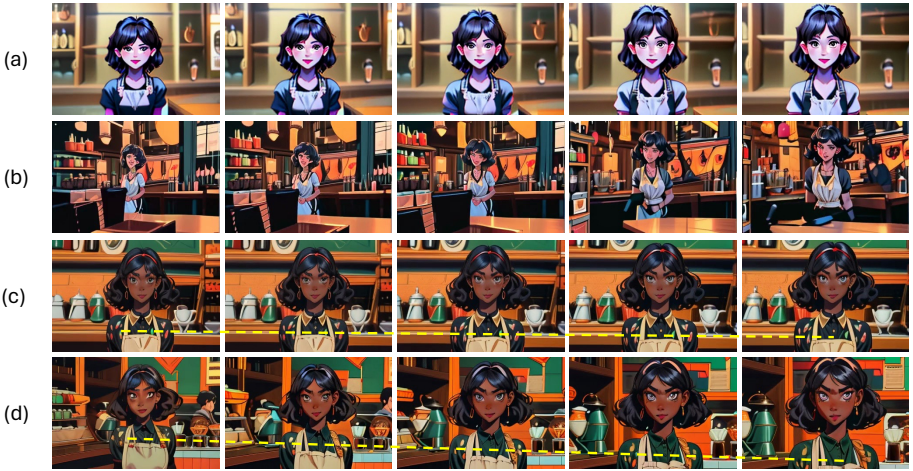


**Fig. 3: Effect of camera encoder architectures.** Row(a) to row(d) represent the results generated with the camera encoder as ControlNet, ControlNet with temporal attention, T2I-Adaptor, T2I-Adaptor with temporal attention, respectively. All the videos are generated using the same text prompt and camera trajectory (zoom-in).

four configurations: ControlNet, T2I-Adaptor, and their temporal attention-enhanced variants.

In this ablation study, we use a personalized T2I backbone ToonYou [9] to generate cartoon characters. According to the Fig. 3, with ControlNet as the camera encoder, the appearance quality is suboptimal. Considering that the ControlNet takes the rgb images as additional input, it may learn some bias towards controlling T2V model to generate contents similar to the training data. This phenomenon is contrary to our objective of creating a camera control model versatile enough to be applicable across various video themes. For the models utilizing the T2I-Adaptor, it is observable that the model with additional temporal attention module exhibits more obvious camera movement, aligning more closely with the intended camera trajectory. Therefore, we chose the T2I-Adaptor with temporal attention module as our camera encoder.

**Injecting camera condition into temporal attention.** We then investigate where the derived camera features should be inserted within the pre-trained U-Net architecture. We conduct three experiments to insert the features into the spatial self attention, spatial cross attention, and temporal attention layers of the U-Net, respectively. The results are presented in the Tab. 2b, indicate that inserting camera features into the temporal attention layers yields better outcomes. This improvement could be attributed to the fact that camera motion typically induces global view changes across frames. Integrating camera poses with the temporal blocks of the LVDM (Latent Video Diffusion Model) resonates with this dynamic nature, thereby enhancing control over camera movements throughout video generation.



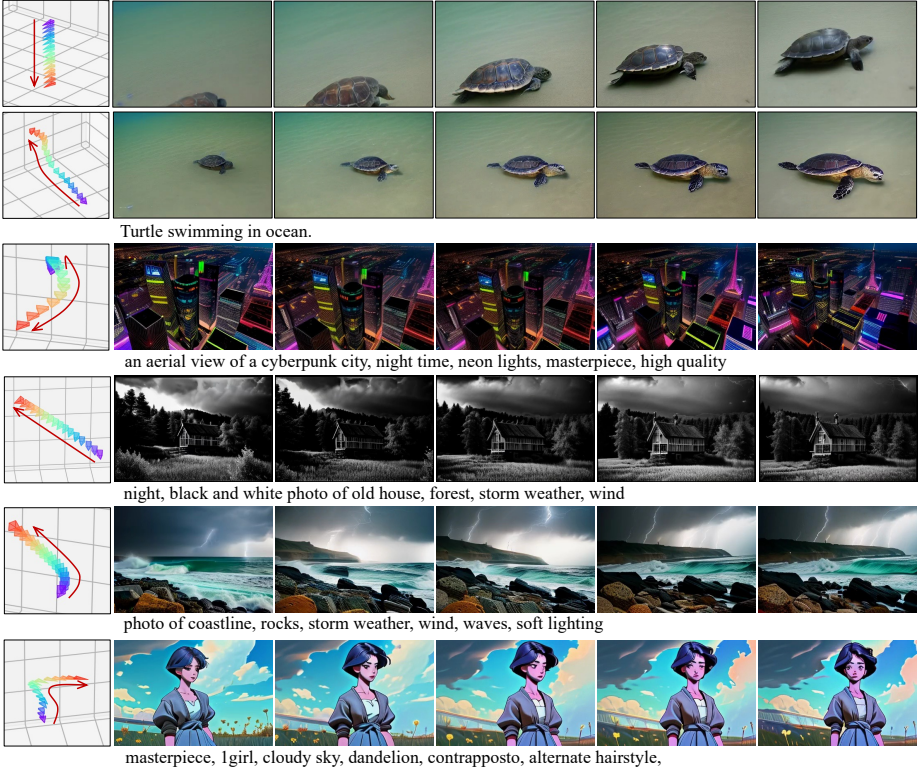


**Fig. 4: Introducing CameraCtrl into text-to-video generation.** The first two rows represent the videos generated by the general T2V model. The following three rows showcase the results of a personalized generator RealisticVision [2]. The video of the last row is produced by another personalized model ToonYou [9].

**Videos with similar appearance distribution and diverse camera help controllability.** To test our argument on dataset selection as discussed in Sec. 3.4, we selected three representative datasets for our experiments. The Objaverse [14] dataset, with camera poses derived from a rendered engine, has the widest distribution of camera poses but has a significantly different appearance from WebVid-10M. For the real-world datasets, compared to MVImageNet, RealEstate10K possesses a more diverse range of camera trajectories.

The results, as shown in the table Tab. 2c, displayed that compared to RealEstate10K, both FID scores and camera errors are significantly higher with MVImageNet. For Objaverse, COLMAP struggles to extract a sufficient number of camera poses to yield meaningful camera error metrics. One possible explanation of this result is that the difference in the dataset appearance may prevent the model from effectively distinguishing between camera pose and appearance, leading to lower video quality (as indicated by poorer FID scores) and inaccurate COLMAP results. Consequently, we ultimately choose for RealEstate10K.

## 4.4 Application of CameraCtrl

**Apply CameraCtrl to different domains of video generation.** As detailed in Sec. 3.3, our camera control model exclusively uses plücker embedding as input, making it independent of the appearance of the training dataset. Besides, as mentioned in Sec. 3.4, we select a dataset with an appearance closely resembling that of the training data of the base T2V model. Benefiting from these design choices, our camera control model can focus solely on learning camera control-related information. This enables its application across various video domains. We demonstrate this versatility with three distinct video domains, results are shown in the Fig. 4. The first and second rows depict natural scenes, illustrating how our method can generate videos using different camera trajectories based on the narrative intent of the same scene. Rows three to five showcase the scenes with styles divergent from the typical reality, such as the buildings of a cyberpunk city, the nature landscape in a black and white video, and coastlines with uncommon color schemes during the stormy weather. The last row represents a video of a cartoon character. Across these varied video generation types, **CameraCtrl** consistently demonstrates effective control over the camera trajectories, showcasing its broad applicability and effectiveness in enhancing video narratives through dynamic camera trajectory control. These results further prove the correctness of our design choices.

**Integrate CameraCtrl with other video control methods.** Thanks to the plug-and-play nature of our method, not only can it be used during the generation processes of different personalized videos, but it can also be integrated with other video generation control techniques together to produce videos. In this session, we utilized SparseCtrl [15], a recent approach that controls the overall video generation by manipulating a few sparse frames. This control can be based on RGB images, sketch maps, or depths. Here, we adopt the RGB encoder and sketch encoder of SparseCtrl, results are shown in Fig. 5. The result of RGB encoder is presented in the first row. It has a high level of consistency between the object rabbit in the generated video and that in the reference frame, and can be conditioned on a given camera trajectory. The results in the second and third rows utilize the sketch encoder of SparseCtrl. It is evident that, based on the provided sketch maps and camera trajectories, the model is capable of generating videos with content that is both reasonable and aligns with the specified camera movements. The successful integration with SparseCtrl further demonstrates the generalization capabilities of **CameraCtrl** and enhances its application prospects.

## 5 Conclusion and Discussion

In this work, we present **CameraCtrl**, a method that addresses the limitations of existing models in precise camera control for video generation. By learning a plug-and-play camera module, **CameraCtrl** enables accurate control over camera viewpoints. Plücker embeddings are adopted as the primary representation of camera parameters, providing a comprehensive description of camera pose information by encoding geometric interpretations. Through a comprehensive study

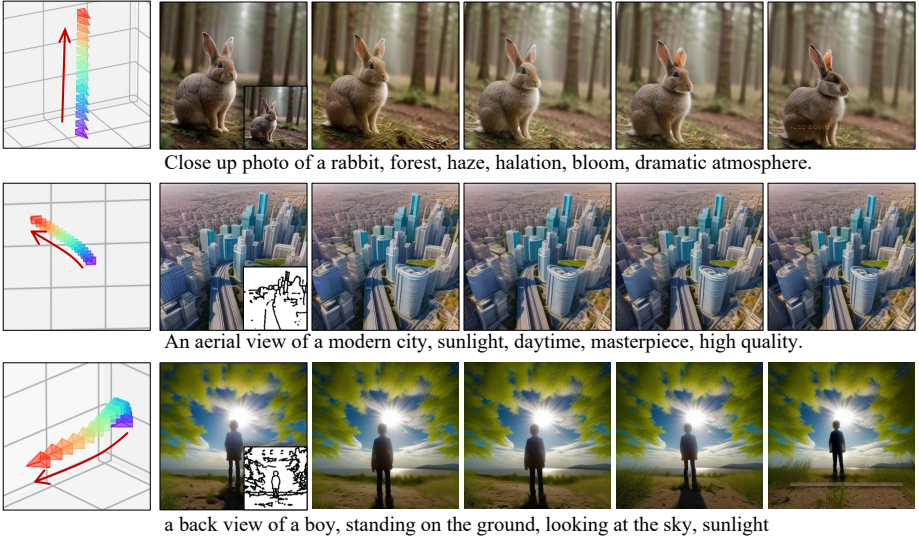


**Fig. 5: Intergrating CameraCtrl into controllable text-to-video generation.** The first row displaces video generated through the combination use of SparseCtrl’s RGB encoder and our method. The last two rows showcase videos produced with the sketch encoder of SparseCtrl alongside our method. Condition images of SparseCtrl are shown in the bottom right corners of the first images for each row. All control signals from SparseCtrl are assigned to the first image.

on training data, it is found that using data with similar appearance to the base model and diverse camera pose distributions, such as RealEstate10K, achieves the best trade-off between generalizability and controllability. Experimental results demonstrate its effectiveness in enhancing the realism of generated videos and enabling customized experiences. Combined with other existing tools, we believe that **CameraCtrl** will inspire further research in the field and contribute to the ongoing evolution of content generation workflows.

**Limitations and future work.** Although **CameraCtrl** has already achieved appealing control of camera, there remains several potential directions to explore. For instance, the generalization of camera control heavily relies on the diversity of training videos. Current choice could meet the demand to some extent while collecting more videos with more complicated camera movement could further improve the controllability. In addition, AnimateDiff [16] provides more than one generator, *i.e.*, a family of text-to-video generators where we evaluate **CameraCtrl**. However, these different generators including others (*e.g.*, VideoCrafter [11], SVD [6]) all adopt U-Net like architecture that combines convolution and attention operations. Regarding transformer generator (*e.g.*, Sora [10]), we believe **CameraCtrl**, as a plug-in module, could be also compatible, which we leave in future to explore.

# CameraCtrl: Enabling Camera Control for Text-to-Video Generation

## Supplementary Material

Hao He<sup>1</sup>, Yinghao Xu<sup>3</sup>, Yuwei Guo<sup>1</sup>,  
Gordon Wetzstein<sup>3</sup>, Bo Dai<sup>2</sup>, Hongsheng Li<sup>1</sup>, and Ceyuan Yang<sup>2</sup>

<sup>1</sup> The Chinese University of Hong Kong  
<sup>2</sup> Shanghai Artificial Intelligence Laboratory  
<sup>3</sup> Stanford University

This supplementary material provides more discussions on data selection, implementation details, additional ablation experiment, and more visual results.

In the visual results, the first image in each row represents the camera trajectory of a video. Each small tetrahedron on this image represents the position and orientation of the camera for one video frame. Its vertex stands for the camera location, while the base represents the imaging plane of the camera. The red arrows indicate the movement of camera **position** but do **not** depict the camera rotation. The camera rotation can be observed through the orientation of the tetrahedrons. **For a clearer understanding of the camera control effects, we highly recommend that readers watch the videos provided in our supplementary file.**

The organization of this supplementary material is as follows: Sec. 1 presents more discussions on the dataset selection process. Sec. 2 gives more implementation details. Sec. 3 depicts one extra ablation study on model architecture. Finally, more visualization results are showcased in Sec. 4.

## 1 More Discussions on Dataset Selection

When selecting the dataset for training our camera control model, we choose three datasets as candidates, Objaverse [14], MVImageNet [53], and RealEstate10K [57].

For the Objaverse dataset, its images are rendered with software like Blender, enabling highly complex camera poses. However, as seen in row one to row three of Fig. 1, its content mainly focuses on objects against white backgrounds. In contrast, the training data for many text-to-video (T2V) models, such as WebVid-10M [4], encompasses both objects and scenes against more intricate backgrounds. This notable difference in appearance can detract from the model’s ability to concentrate solely on learning camera control. For MVImageNet data, it has some backgrounds and complex individual camera trajectories. Nevertheless, as demonstrated in the row four to row six of Fig. 1, most of the camera trajectories in the MVImageNet are horizontal rotations. Thus, its camera trajectories lack diversity, which could lead the model to learn a fixed pattern. Regarding RealEstate10K data, as shown in the row seven to row nine of Fig. 1, it features both indoor and outdoor scenes and objects. Besides, each camera

trajectory in RealEstate10K is complex and there exists a considerable variety among different camera trajectories. Therefore, we choose the RealEstate10K dataset to train our camera control model.

## 2 More Implementation Details

**Training.** We use the LAVIS [28] to generate the text prompts for each video clip of the RealEstate10K dataset. For each training sample, we sample 16 images from one video clip with the sample stride equal to 8, then resize their resolution to  $256 \times 384$ . After that, we use the random horizontal flip for both images and poses with a 50 percent probability. We use a *linear* beta schedule, where  $\beta_{start} = 0.00085$ ,  $\beta_{end} = 0.012$ , and  $T = 1000$ . To let the camera control model better focus on learning camera poses, similar to AnimateDiff [16], we first train an image LoRA on the images of RealEstate10K dataset. Then, based on the T2V model enhanced with LoRA, we train the camera control model. Note that, after the camera control model is trained, the image LoRA can be removed. **Inference.** By utilizing structure-from-motion methods such as COLMAP [41], along with existing videos, we can extract the camera trajectory within a video. This extracted camera trajectory can then be fed into our camera control model to generate videos with similar camera movements. Additionally, we can also design custom camera trajectories to produce videos with desired camera movement. During the inference, we use different guidance scales for different domains’ videos and adopt a constant denoise step 25 for all the videos.

## 3 Extra Ablation Study

**Injecting camera features into both encoder and decoder of U-Net.** In the vanilla T2I-Adaptor [33], the extracted control features are only fed into the encoder of U-Net. In this part, we explore whether injecting the camera features to both U-Net encoder and decoder could result in performance improvements. The experiment results are shown in Tab. 1. The improvements of **TransErr** and **RotErr** indicate that, compared to only sending camera features to U-Net encoder, injecting the camera features to both the encoder and decoder enhances camera control accuracy. This result could be attributed to the fact that similar to text embedding, the plücker embedding inherently lacks structural information. Such that, this integrating choice allows the U-Net model to leverage camera features more effectively. Therefore, we ultimately choose to feed the camera features to both the encoder and decoder of the U-Net.

## 4 More Visualization results

This section provides additional visualization results of **CameraCtrl**. All the results are generated using the **same** camera control model.

**Table 1:** Ablation study of the camera feature injection place.

Injection Place	FID $\downarrow$	TransErr $\downarrow$	RotErr $\downarrow$
U-Net Encoder	<b>99.0</b>	13.82	1.45
<b>U-Net Encoder + Decoder</b>	100.4	<b>12.91</b>	<b>1.25</b>

#### 4.1 Visualization results of various domain videos

**Visual results of RealEstate10K domain.** First, with the aforementioned image LoRA model trained on RealEstate10K dataset, and using captions and camera trajectories from RealEstate10K, **CameraCtrl** is capable of generating videos within the RealEstate10K domain. Results are shown in Fig. 2, the camera movement in generated videos closely follows the control camera poses, and the generated contents are also aligned with the text prompts.

**Visual results of original T2V model domain.** We choose the AnimateDiff V3 [16] as our video generation base model, which is trained on the WebVid-10M dataset. Without the RealEstate10K image LoRA, **CameraCtrl** can be used to control the camera poses during the video generation of natural objects and scenes. As shown in Fig. 3, with the same text prompts, taking different camera trajectories as input, **CameraCtrl** can generate almost the same scene, and closely follows the camera trajectories. Besides, Fig. 4 shows more visual results of natural objects and scenes.

**Visual results of some personalized video domain.** By replacing the image generator backbone of T2V model with some personalized generator, **CameraCtrl** can be used to control the camera poses in the personalized videos. With the personalized generator RealisticVision [2], Fig. 5 showcases the results of some stylized objects and scenes, like some uncommon color schemes in the landscape and coastline. Besides, with another personalized generator ToonYou [9], **CameraCtrl** can be used in the cartoon character video generation process. Some results are shown in Fig. 6. Note that, in both domains, the camera trajectories in the generated videos closely follow the control camera poses.

#### 4.2 Integrating CameraCtrl with other video control method

Fig. 7 gives some generated results by integrating the **CameraCtrl** with another video control method SparseCtrl [15]. The content of the generated videos follows the input RGB image or sketch map closely, while the camera trajectories of the videos also effectively align with the conditioned camera trajectories.



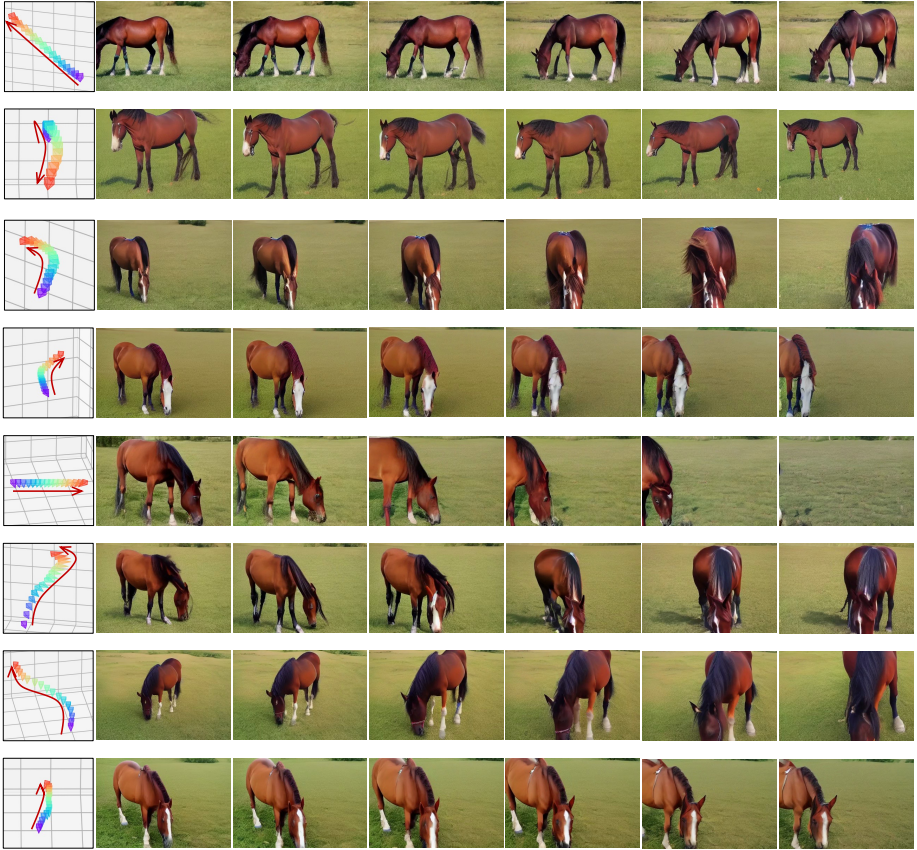


**Fig. 1: Samples of different datasets.** Row one to row three are samples from Objaverse dataset, which has random camera poses for each rendered image. Row four to row six show the samples from the MVImageNet dataset. Samples of the RealEstate10K dataset are presented from row seven to row nine.





**Fig. 2: RealEstate10K visual results.** The video generation results of CameraCtrl. The control camera trajectories and captions are both from RealEstate10K test set.



A horse is eating grass on the grassland.

**Fig. 3: Using CameraCtrl on the same caption and different camera trajectories.** The camera control results of CameraCtrl. Camera trajectories are from RealEstate10K test set, all videos utilize the same text prompts.

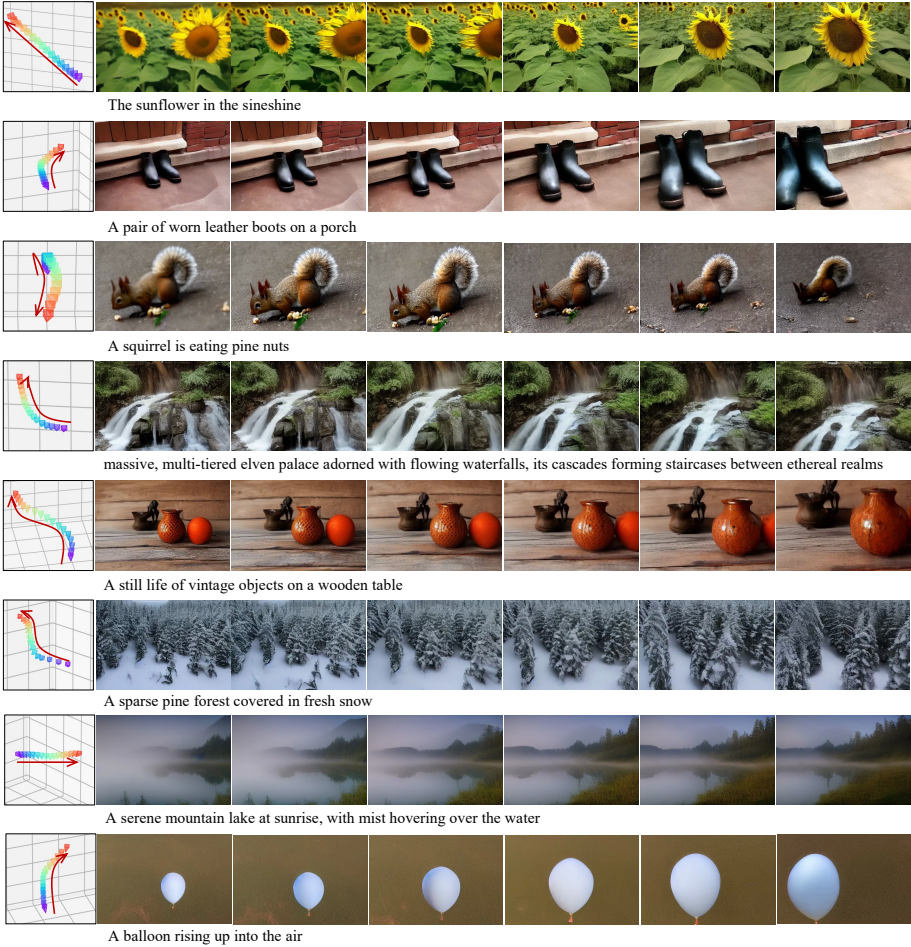


**Fig. 4: Visual results of natural objects and scenes.** The natural video generation results of CameraCtrl. CameraCtrl can be used to control the camera poses during the video generation process of natural objects and scenes.



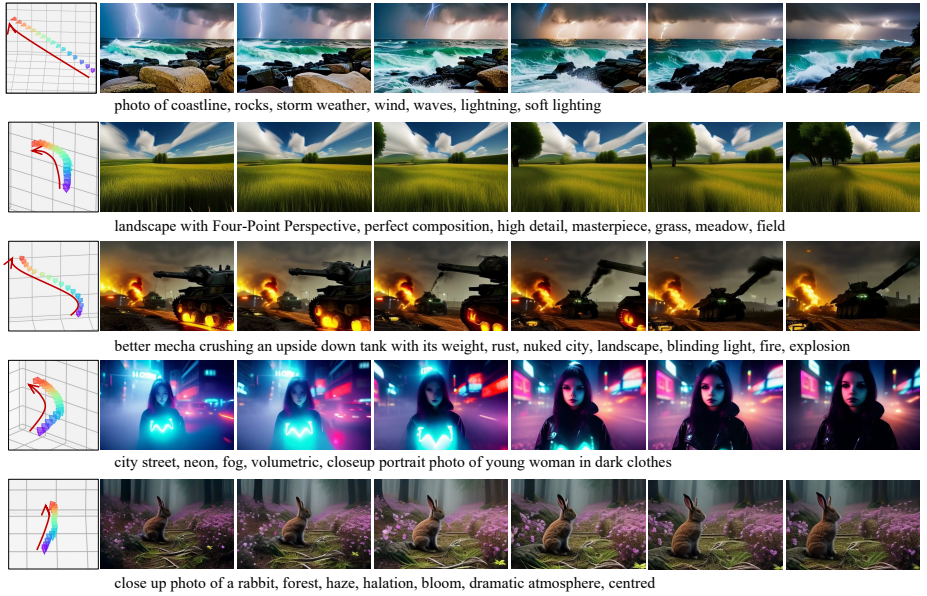


**Fig. 5: Visual results of stylized objects and scenes.** With the personalized generator RealisticVision [2], CameraCtrl can be used in the video generation process of stylized videos.

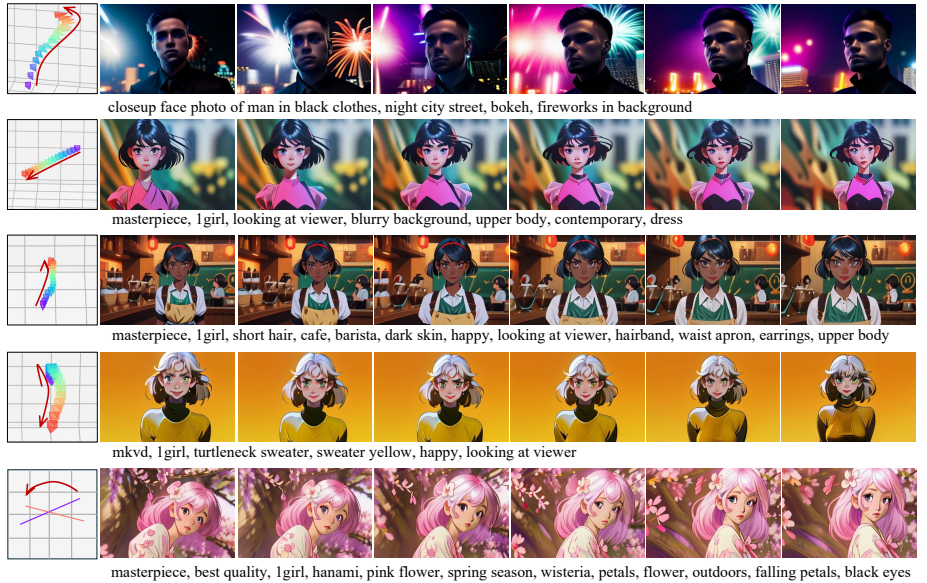


**Fig. 6: Visual results of cartoon characters.** With the personalized generator ToonYou [9], CameraCtrl can be used in the video generation process of cartoon character videos.

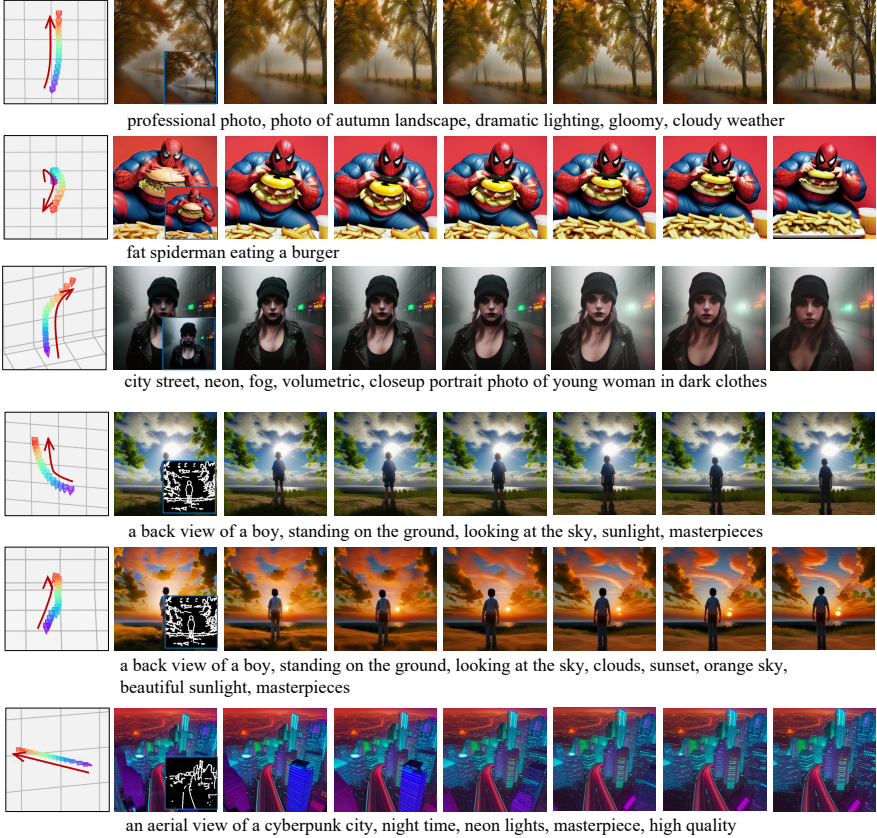


**Fig. 7: Integrating CameraCtrl with other video generation control methods.** Row one to row three express the results by integrating the CameraCtrl with RGB encoder of SparseCtrl [15], and row four to row six, shows videos produced with the sketch encoder of SparseCtrl. The condition RGB images and sketch maps are shown in the bottom right corners of the second images for each row. Note that, the camera trajectory of the last row is zoom-in.

## References

1. <http://www.boris-belousov.net/2016/12/01/quat-dist/> 8
2. (2023), <https://civitai.com/models/4201/realistic-vision-v20> 12, 17, 22
3. Bain, M., Nagrani, A., Varol, G., Zisserman, A.: Frozen in time: A joint video and image encoder for end-to-end retrieval. In: Proceedings of the IEEE/CVF International Conference on Computer Vision. pp. 1728–1738 (2021) 3
4. Bain, M., Nagrani, A., Varol, G., Zisserman, A.: Frozen in time: A joint video and image encoder for end-to-end retrieval. In: Proceedings of the IEEE/CVF International Conference on Computer Vision. pp. 1728–1738 (2021) 7, 15
5. Bar-Tal, O., Chefer, H., Tov, O., Herrmann, C., Paiss, R., Zada, S., Ephrat, A., Hur, J., Li, Y., Michaeli, T., et al.: Lumiere: A space-time diffusion model for video generation. arXiv preprint arXiv:2401.12945 (2024) 3
6. Blattmann, A., Dockhorn, T., Kulal, S., Mendelevitch, D., Kilian, M., Lorenz, D., Levi, Y., English, Z., Voleti, V., Letts, A., et al.: Stable video diffusion: Scaling latent video diffusion models to large datasets. arXiv preprint arXiv:2311.15127 (2023) 14
7. Blattmann, A., Rombach, R., Ling, H., Dockhorn, T., Kim, S.W., Fidler, S., Kreis, K.: Align your latents: High-resolution video synthesis with latent diffusion models. In: Proceedings of the IEEE/CVF Conference on Computer Vision and Pattern Recognition. pp. 22563–22575 (2023) 1, 4
8. Blattmann, A., Rombach, R., Ling, H., Dockhorn, T., Kim, S.W., Fidler, S., Kreis, K.: Align your latents: High-resolution video synthesis with latent diffusion models. In: Proceedings of the IEEE/CVF Conference on Computer Vision and Pattern Recognition. pp. 22563–22575 (2023) 3
9. Bradcatt: Toonyou, <https://civitai.com/models/30240/toonyou> (2023), <https://civitai.com/models/30240/toonyou> 11, 12, 17, 22
10. Brooks, T., Peebles, B., Holmes, C., DePue, W., Guo, Y., Jing, L., Schnurr, D., Taylor, J., Luhman, T., Luhman, E., Ng, C., Wang, R., Ramesh, A.: Video generation models as world simulators (2024), <https://openai.com/research/video-generation-models-as-world-simulators> 3, 14
11. Chen, H., Xia, M., He, Y., Zhang, Y., Cun, X., Yang, S., Xing, J., Liu, Y., Chen, Q., Wang, X., Weng, C., Shan, Y.: Videocrafter1: Open diffusion models for high-quality video generation (2023) 3, 14
12. Chen, T.S., Lin, C.H., Tseng, H.Y., Lin, T.Y., Yang, M.H.: Motion-conditioned diffusion model for controllable video synthesis. arXiv preprint arXiv:2304.14404 (2023) 1
13. Chen, W., Wu, J., Xie, P., Wu, H., Li, J., Xia, X., Xiao, X., Lin, L.: Control-a-video: Controllable text-to-video generation with diffusion models. arXiv preprint arXiv:2305.13840 (2023) 3
14. Deitke, M., Schwenk, D., Salvador, J., Weihs, L., Michel, O., VanderBilt, E., Schmidt, L., Ehsani, K., Kembhavi, A., Farhadi, A.: Objaverse: A universe of annotated 3d objects. In: Proceedings of the IEEE/CVF Conference on Computer Vision and Pattern Recognition. pp. 13142–13153 (2023) 7, 12, 15
15. Guo, Y., Yang, C., Rao, A., Agrawala, M., Lin, D., Dai, B.: Sparsectrl: Adding sparse controls to text-to-video diffusion models. arXiv preprint arXiv:2311.16933 (2023) 2, 3, 10, 13, 17, 23
16. Guo, Y., Yang, C., Rao, A., Wang, Y., Qiao, Y., Lin, D., Dai, B.: Animatediff: Animate your personalized text-to-image diffusion models without specific tuning. arXiv preprint arXiv:2307.04725 (2023) 1, 2, 3, 4, 6, 8, 9, 14, 16, 17

17. Gupta, A., Yu, L., Sohn, K., Gu, X., Hahn, M., Fei-Fei, L., Essa, I., Jiang, L., Lezama, J.: Photorealistic video generation with diffusion models. arXiv preprint arXiv:2312.06662 (2023) **3**
18. He, Y., Yang, T., Zhang, Y., Shan, Y., Chen, Q.: Latent video diffusion models for high-fidelity video generation with arbitrary lengths. arXiv preprint arXiv:2211.13221 (2022) **3**
19. Ho, J., Chan, W., Saharia, C., Whang, J., Gao, R., Gritsenko, A., Kingma, D.P., Poole, B., Norouzi, M., Fleet, D.J., et al.: Imagen video: High definition video generation with diffusion models. arXiv preprint arXiv:2210.02303 (2022) **1**
20. Ho, J., Jain, A., Abbeel, P.: Denoising diffusion probabilistic models. *Advances in Neural Information Processing Systems* **33**, 6840–6851 (2020) **3**
21. Ho, J., Salimans, T., Gritsenko, A., Chan, W., Norouzi, M., Fleet, D.J.: Video diffusion models. arXiv:2204.03458 (2022) **3, 4**
22. Hong, W., Ding, M., Zheng, W., Liu, X., Tang, J.: Cogvideo: Large-scale pretraining for text-to-video generation via transformers. arXiv preprint arXiv:2205.15868 (2022) **3**
23. Hu, E.J., Shen, Y., Wallis, P., Allen-Zhu, Z., Li, Y., Wang, S., Wang, L., Chen, W.: Lora: Low-rank adaptation of large language models. arXiv preprint arXiv:2106.09685 (2021) **4**
24. Hu, L., Gao, X., Zhang, P., Sun, K., Zhang, B., Bo, L.: Animate anyone: Consistent and controllable image-to-video synthesis for character animation. arXiv preprint arXiv:2311.17117 (2023) **3**
25. Karras, J., Holynski, A., Wang, T.C., Kemelmacher-Shlizerman, I.: Dreampose: Fashion video synthesis with stable diffusion. In: *Proceedings of the IEEE/CVF International Conference on Computer Vision*. pp. 22680–22690 (2023) **3**
26. Khachatryan, L., Movsisyan, A., Tadevosyan, V., Henschel, R., Wang, Z., Navasardyan, S., Shi, H.: Text2video-zero: Text-to-image diffusion models are zero-shot video generators. *IEEE International Conference on Computer Vision (ICCV)* (2023) **3**
27. Kondratyuk, D., Yu, L., Gu, X., Lezama, J., Huang, J., Hornung, R., Adam, H., Akbari, H., Alon, Y., Birodkar, V., et al.: Videopoet: A large language model for zero-shot video generation. arXiv preprint arXiv:2312.14125 (2023) **3**
28. Li, D., Li, J., Le, H., Wang, G., Savarese, S., Hoi, S.C.: LAVIS: A one-stop library for language-vision intelligence. In: *Proceedings of the 61st Annual Meeting of the Association for Computational Linguistics (Volume 3: System Demonstrations)*. pp. 31–41. Association for Computational Linguistics, Toronto, Canada (Jul 2023), <https://aclanthology.org/2023.acl-demo.3> **16**
29. Li, Z., Dekel, T., Cole, F., Tucker, R., Snively, N., Liu, C., Freeman, W.T.: Learning the depths of moving people by watching frozen people. In: *Proceedings of the IEEE/CVF conference on computer vision and pattern recognition*. pp. 4521–4530 (2019) **7**
30. Liu, A., Tucker, R., Jampani, V., Makadia, A., Snively, N., Kanazawa, A.: Infinite nature: Perpetual view generation of natural scenes from a single image. In: *Proceedings of the IEEE/CVF International Conference on Computer Vision*. pp. 14458–14467 (2021) **7**
31. Ma, X., Wang, Y., Jia, G., Chen, X., Liu, Z., Li, Y.F., Chen, C., Qiao, Y.: Latte: Latent diffusion transformer for video generation. arXiv preprint arXiv:2401.03048 (2024) **3**
32. Ma, Y., He, Y., Cun, X., Wang, X., Shan, Y., Li, X., Chen, Q.: Follow your pose: Pose-guided text-to-video generation using pose-free videos. arXiv preprint arXiv:2304.01186 (2023) **1**



33. Mou, C., Wang, X., Xie, L., Wu, Y., Zhang, J., Qi, Z., Shan, Y., Qie, X.: T2i-adapter: Learning adapters to dig out more controllable ability for text-to-image diffusion models. arXiv preprint arXiv:2302.08453 (2023) [5](#), [6](#), [16](#)
34. Ni, H., Shi, C., Li, K., Huang, S.X., Min, M.R.: Conditional image-to-video generation with latent flow diffusion models. In: Proceedings of the IEEE/CVF Conference on Computer Vision and Pattern Recognition. pp. 18444–18455 (2023) [3](#)
35. Peebles, W., Xie, S.: Scalable diffusion models with transformers. In: Proceedings of the IEEE/CVF International Conference on Computer Vision. pp. 4195–4205 (2023) [3](#)
36. Rombach, R., Blattmann, A., Lorenz, D., Esser, P., Ommer, B.: High-resolution image synthesis with latent diffusion models. In: Proceedings of the IEEE/CVF Conference on Computer Vision and Pattern Recognition. pp. 10684–10695 (2022) [3](#)
37. Ruan, L., Ma, Y., Yang, H., He, H., Liu, B., Fu, J., Yuan, N.J., Jin, Q., Guo, B.: Mm-diffusion: Learning multi-modal diffusion models for joint audio and video generation. In: Proceedings of the IEEE/CVF Conference on Computer Vision and Pattern Recognition. pp. 10219–10228 (2023) [1](#)
38. Ruan, L., Ma, Y., Yang, H., He, H., Liu, B., Fu, J., Yuan, N.J., Jin, Q., Guo, B.: Mm-diffusion: Learning multi-modal diffusion models for joint audio and video generation. In: Proceedings of the IEEE/CVF Conference on Computer Vision and Pattern Recognition. pp. 10219–10228 (2023) [3](#)
39. Ruiz, N., Li, Y., Jampani, V., Pritch, Y., Rubinstein, M., Aberman, K.: Dream-booth: Fine tuning text-to-image diffusion models for subject-driven generation. In: Proceedings of the IEEE/CVF Conference on Computer Vision and Pattern Recognition. pp. 22500–22510 (2023) [1](#)
40. Ruiz, N., Li, Y., Jampani, V., Pritch, Y., Rubinstein, M., Aberman, K.: Dream-booth: Fine tuning text-to-image diffusion models for subject-driven generation. In: Proceedings of the IEEE/CVF Conference on Computer Vision and Pattern Recognition. pp. 22500–22510 (2023) [3](#)
41. Schönberger, J.L., Frahm, J.M.: Structure-from-motion revisited. In: Conference on Computer Vision and Pattern Recognition (CVPR) (2016) [7](#), [16](#)
42. Singer, U., Polyak, A., Hayes, T., Yin, X., An, J., Zhang, S., Hu, Q., Yang, H., Ashual, O., Gafni, O., et al.: Make-a-video: Text-to-video generation without text-video data. arXiv preprint arXiv:2209.14792 (2022) [4](#)
43. Sitzmann, V., Rezhikov, S., Freeman, B., Tenenbaum, J., Durand, F.: Light field networks: Neural scene representations with single-evaluation rendering. *Advances in Neural Information Processing Systems* **34**, 19313–19325 (2021) [2](#), [5](#)
44. Song, J., Meng, C., Ermon, S.: Denoising diffusion implicit models. arXiv preprint arXiv:2010.02502 (2020) [3](#)
45. Wang, X., Yuan, H., Zhang, S., Chen, D., Wang, J., Zhang, Y., Shen, Y., Zhao, D., Zhou, J.: Videocomposer: Compositional video synthesis with motion controllability. *Advances in Neural Information Processing Systems* **36** (2024) [1](#)
46. Wang, Z., Yuan, Z., Wang, X., Chen, T., Xia, M., Luo, P., Shan, Y.: Motionctrl: A unified and flexible motion controller for video generation. arXiv preprint arXiv:2312.03641 (2023) [2](#), [4](#), [8](#), [9](#)
47. Wu, J.Z., Ge, Y., Wang, X., Lei, S.W., Gu, Y., Shi, Y., Hsu, W., Shan, Y., Qie, X., Shou, M.Z.: Tune-a-video: One-shot tuning of image diffusion models for text-to-video generation. In: Proceedings of the IEEE/CVF International Conference on Computer Vision. pp. 7623–7633 (2023) [1](#)

48. Xing, J., Xia, M., Liu, Y., Zhang, Y., Zhang, Y., He, Y., Liu, H., Chen, H., Cun, X., Wang, X., et al.: Make-your-video: Customized video generation using textual and structural guidance. arXiv preprint arXiv:2306.00943 (2023) [1](#)
49. Xu, Z., Zhang, J., Liew, J.H., Yan, H., Liu, J.W., Zhang, C., Feng, J., Shou, M.Z.: Magicanimate: Temporally consistent human image animation using diffusion model. arXiv preprint arXiv:2311.16498 (2023) [3](#)
50. Yang, S., Hou, L., Huang, H., Ma, C., Wan, P., Zhang, D., Chen, X., Liao, J.: Direct-a-video: Customized video generation with user-directed camera movement and object motion. arXiv preprint arXiv:2402.03162 (2024) [4](#), [9](#)
51. Ye, H., Zhang, J., Liu, S., Han, X., Yang, W.: Ip-adapter: Text compatible image prompt adapter for text-to-image diffusion models. arXiv preprint arXiv:2308.06721 (2023) [5](#)
52. Yin, S., Wu, C., Liang, J., Shi, J., Li, H., Ming, G., Duan, N.: Dragmuwa: Fine-grained control in video generation by integrating text, image, and trajectory. arXiv preprint arXiv:2308.08089 (2023) [1](#)
53. Yu, X., Xu, M., Zhang, Y., Liu, H., Ye, C., Wu, Y., Yan, Z., Zhu, C., Xiong, Z., Liang, T., et al.: Mvimnet: A large-scale dataset of multi-view images. In: Proceedings of the IEEE/CVF Conference on Computer Vision and Pattern Recognition. pp. 9150–9161 (2023) [7](#), [15](#)
54. Zhang, L., Rao, A., Agrawala, M.: Adding conditional control to text-to-image diffusion models. In: Proceedings of the IEEE/CVF International Conference on Computer Vision. pp. 3836–3847 (2023) [5](#), [6](#), [10](#)
55. Zhang, S., Wang, J., Zhang, Y., Zhao, K., Yuan, H., Qin, Z., Wang, X., Zhao, D., Zhou, J.: I2vgen-xl: High-quality image-to-video synthesis via cascaded diffusion models. arXiv preprint arXiv:2311.04145 (2023) [3](#)
56. Zhang, Y., Wei, Y., Jiang, D., Zhang, X., Zuo, W., Tian, Q.: Controlvideo: Training-free controllable text-to-video generation. arXiv preprint arXiv:2305.13077 (2023) [3](#)
57. Zhou, T., Tucker, R., Flynn, J., Fyffe, G., Snavely, N.: Stereo magnification: Learning view synthesis using multiplane images. arXiv preprint arXiv:1805.09817 (2018) [3](#), [7](#), [15](#)